Study on Humanoid Robot Systems:
an Energy Approach

L. De Michieli[1], F. Nori[1], A. Pini Prato[2], G. Sandini[1,3]

[1]RBCS Department, Fondazione Istituto Italiano di Tecnologia, Italy, *lorenzo.demichieli@iit.it*, *francesco.nori@iit.it*,
[2]DIMSET Department, Università di degli Studi di Genova, Italy, *salbi@unige.it*
[3]DIST-Lira Lab, Università di degli Studi di Genova, Italy, *giulio.sandini@iit.it*

Abstract— **This work is about the energy analysis of a humanoid robotic arm, seen as complex energy chain. The problem of energy efficiency in robotics is becoming crucial in order to make robots achieve an increasing number of tasks in cooperation with humans or in substitution of them. Our approach consists in representing the humanoid robot as an isolated energy systems. We developed a simulation platform suitable for modelling the kinematics, dynamics, and energy balances of a real humanoid robotic arm. The model was validated by an accurate comparison with the real robot. Then, we performed a first compared study of the motion dynamics of the simulated robot arm and the energy flows which crossed its energy converters, with respect to a set of different motion control strategies. Moreover, we conducted a preliminary investigation on the possibility of saving and recovering energy during robot motion.**

I. INTRODUCTION

It is expected that humanoid robots will be used to accomplish a large number of tasks, for example, high risk duties, such as exploration, search and rescue, security, operations in hostile environments such as space or underwater [1]. To attain these goals, some fundamental characteristics of robots, such as energy efficiency, should be enhanced [2], [3], [4].

This work intends to provide an energy analysis of a state of art humanoid robot [11] according to some of the methodologies which derive from research on distributed energy systems and energy converters, by developing suitable instruments and methods [5], [6], [7]. According to our approach, humanoid robots are represented as isolated energy systems. From this perspective, they can be schematized like energy chains. They are constituted of a number of energy converters which are interconnected so as to produce the expected task.

Typically, humanoid robots are equipped with at least one primary converter (for instance, a battery or an internal combustion engine), which provides the energy required by the robot, thus determining the initial point of the energy chain. In general, after the principal energy converter, other converters aimed at transforming the electric energy into mechanical energy are connected. Usually they are electric motors. At the end of the energy chain there are those converters that have direct interaction with the environment, that is, the robot workspace. They are the robot actuators such as tactile sensors, manipulators, pincers, cameras, human-like hands. Finally, all the energy converters are interconnected within a power distribution net. A central control unit is expected to manage the distribution net and to dispatch the appropriate power to each single converter in order to carry out the desired mission (i.e. goal oriented task).

Similar to more common models of isolated energy chain, (for example automobiles, aircraft or ships), humanoid robots are obliged to alternate working cycles: they produce periods of usefulness followed by periods of inactivity. The problem of the autonomy, and therefore of energy efficiency, of humanoid robots is remarkable [8], especially in view of assigning them increasingly complex tasks. Besides the search for energy converters which may provide increased performance in terms of capacity, duration and quality of energy supply, a solution can be carried out studying the structural characteristics as well as the dynamics of the robot system, aimed at minimizing its energy consumption with respect to a given mission [2], [9], [12]. Accordingly, the energy chain must be analysed in terms of single converters, especially concerning effects that the possible variations of typology and topography of the intermediate converters produce on the primary converter, for a given task. Moreover, in case the structure of the robot is determined in terms of configuration and category of the actuators, and the desired mission is identified, it is important to conduct an energy analysis of the effects of the motion controls and the cognitive process which regulate the robot functioning. Indeed, the overall efficiency of the robot for a determined mission is not due only to the efficiency of its energy chain, but it is also strongly dependent on the actions that the robot decides to carry out [8] [10].

This type of analysis requires the definition and use of an appropriate physical model that resolves the dynamics of each converter, including the effects of both the internal and the external forces acting on it, such as friction, gravity, inertial effects. The characterization of the energy chain duty cycles allows to study the efficiencies of the energy chain, and to identify energy losses and uses with respect to the global duty cycle. As an example, it is possible to calculate the backward energy flows occurring when the robot arm moves under the effect of gravity, or when it is driven by external forces.

We believe that the correlation of the energy aspects of a humanoid robot with its motion dynamics and its control strategies can represent an effective approach to individuate an energy efficient design of the system.

II. OBJECTIVES

Our primary objective is to develop a simulation platform suitable for modelling the kinematics, dynamics, and energy balance of a real humanoid robotic arm. We want to provide a flexible simulator that allow us to reproduce the elements of the robot energy chain in terms of mechanical and electrical components, and to simulate a large number of motion control strategies.

A further aim is to present a correlation between the motion dynamics of the robot arm and the energy flows which cross its constituents, with respect to a set of different motion control strategies. In particular, three motion control logics have been developed and compared with the one which currently drives the real robotic arm. The model of the arm, under the supervision of these four controls, has been involved in a series of simulated goal oriented tasks in order to obtain a study of the dynamics, the kinematics and the energy related parameters of the converters as well as the whole energy chain. From a broader point of view, the work aims at investigating the possibility to save or even recover energy during robot motion.

III. DESCRIPTION OF ROBOT JAMES

James is a humanoid robotic platform which is developed by the University of Genoa in collaboration with the Italian Institute of Technology.

It has been designed by considering an object manipulation scenario and by explicitly taking into account embodiment, interaction and the exploitation of smart design solutions. The robot is equipped with moving eyes, neck, arm and hand, and a rich set of sensors, enabling proprioceptive, kinesthetic, tactile and visual sensing.
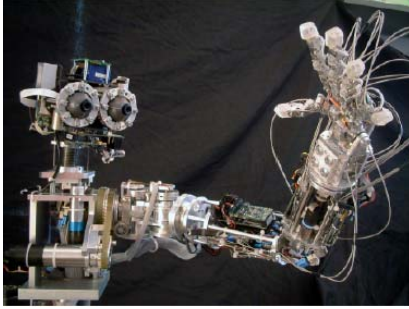

Fig. 1 The humanoid robot James at IIT

James consists of 22 Degrees of Freedom (DOF), actuated by a total of 23 motors, whose torque is transmitted to the joints by belts and stainless-steel tendons. The head is equipped with two eyes, which can pan and tilt independently (4 DOFs), and is mounted on a 3-DOF neck, which allows the movement of the head as needed in the 3D rotational space.

The arm has 7 DOFs: three of them are located in the shoulder, one in the elbow and three in the wrist.

The hand has five fingers. Each of them has three joints (flexion/extension of the distal, middle and proximal phalanxes). The overall size of James is that of a ten-year-old boy, with the appropriate proportions for a total weight of

about 9 kg: 2 kg the head, 4 kg the torso and 3 kg arm and hand together.

The robot arm, which is the object of the simulation described herein, is basically composed of four main parts: the shoulder, the upper arm, the forearm, and the hand. In the following a brief description of the single mechanical parts is given.

A. The shoulder

The design of the tendon driven shoulder was developed with the main intent of allowing a wide range of movements. The current design, consists of three successive rotations φ^J, which we may conventionally call pitch φ_p^J, yaw φ_y^J, and roll φ_r^J respectively (Fig. 2). The abduction (yaw) rotation is divided along two mechanically coupled joints having rotation corresponding to a sequence of two identical rotations $\varphi_{y/2}^J$ around two parallel axes. Indeed, a mechanical tight coupling forces the two angles of rotation to be equal. This 'ad hoc' solution allows the arm to gain an impressive range of movement (pitch $\cong 360°$, yaw $\cong 180°$, roll $\cong 180°$).
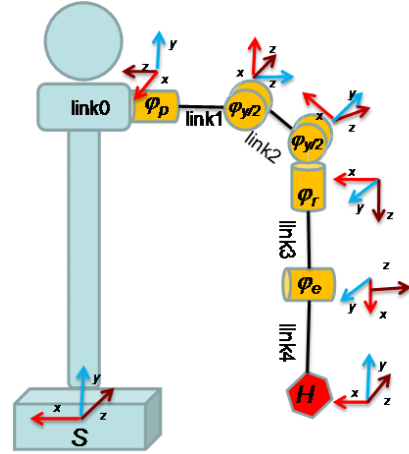

Fig. 2 The kinematic chain of James's arm. The systems of reference herein reported are chosen according to the Denavit Hartemberg notation.

James arm is actuated by a set of 4 DC Faulhaber motors which we will call M1, M2, M3, M4. Each motor is equipped with a planetary gearhead of nominal reduction ratio comprised between 66 and 246. Moreover, each motor is coupled with an incremental magnetic encoder in order to provide a feedback of the shaft position during the motion, hence providing the possibility to calculate the relative position of the links. Actuation is achieved by exploiting the design of tendons and pulleys.

A table of the motors specifications is reported herein:

TABLE I
MOTORS MODELS DRIVING THE 4 DOF ROBOT ARM

#	DC MOTOR (FAULHABER)	GEARHEAD (FAULHABER)
M1	3242G012CR	32/3, reduction ratio: 246:1
M2	3242G012CR	32/3, reduction ratio: 246:1
M3	2342S012CR	26/1, reduction ratio: 66:1
M4	2224U012SR	23/1, reduction ratio: 246:1

The first three motors are lodged inside the torso, displaced horizontally. They are dedicated to the actuation of the shoulder (links 1, 2) and the upper arm (link 3). Both motor M1 and motor M2 are connected link 1 by means of rubber-toothed belts. Motor M3 is connected to link 3 by one ribbon belt collaborating with tendons and pulleys. Motor M4 is positioned within the aluminium frame of the upper arm.

While the forearm rotation φ_e^J about the elbow axis is actuated by the motor M4 only, the rotations of the first three links about the yaw, pitch, and roll axis, are caused by the simultaneous actuation of the motors M1, M2, and M3.

Indicating with $(\varphi_p^M \; \varphi_y^M \; \varphi_r^M \; \varphi_e^M)$ the shafts' angles of the motors M1, M2, M3, M4, the relation between these angles and the rotation angles yaw pitch and roll can be written as:

(1.1) $$\left[\varphi_p^J \; \varphi_y^J \; \varphi_r^J\right]^T = D\left[\varphi_p^M \; \varphi_y^M \; \varphi_r^M\right]^T$$

where

(1.2) $$D = 0.555\begin{bmatrix} \frac{1}{246} & 0 & 0 \\ -\frac{2}{246} & \frac{2}{246} & 0 \\ \frac{1}{246} & \frac{2}{246} & \frac{1}{66} \end{bmatrix}$$

The numerical values of D derives from the values of the coupling factors between the position of motors and the position of links and the reduction ratios of the gearboxes.

IV. DESCRIPTION OF THE SIMULATOR

The simulator has been designed with the aim of being fully configurable with respect to the mechanical and electrical specifications, so that any change in the kinematic of the robot, in the motors and in the robot dynamical characteristics can be easy to implement and managed.
The simulator can be divided in the following 5 groups:

A: the mechanical apparatus;
B: the DC motors / mechanical transmission;
C: the motion control strategies module;
D: the energy analysis module.

The simulator requires the use of two different software packages: a professional mobile robot simulation software named 'Webots' and the well known 'Matlab' package. These two software have been linked by means of tcp/ip like communication protocol in order to obtain one single simulation environment. The Mechanical apparatus (A) and part of the Motion control (C) have been developed by using Webots. The DC motors (B) and the Energy analysis module (D) have been developed in Matlab code, whereas motor controls and most of the custom physics simulation libraries have been implemented in C language.

A. The Mechanical Apparatus

The 4 DOF (Degrees of Freedom) mechanical apparatus (A) has been reproduced by using Webots together with ad hoc C language plug ins in order to overcome Webots limitations. These resides in the difficulty of modelling group of motors collaborating on the same joint, as well as the mechanical coupling of the shoulder yaw movement previously described.

The model has been schematised as a set of rigid multibody system consisting of a set of rigid objects joined together by joints and ending with an actuator (the hand) or end-effector.

The whole kinematic chain of the arm has 4 DOF and is mechanically connected to the upper torso from one side, and to the other side it is rigidly attached to the robot hand. The following Fig. 3 shows the simulated James layout.
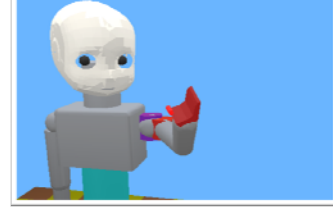

Fig. 3 Graphical representation of James model. The dynamical and energy calculation is confined to the 4DOF arm.

B. The DC Motors and the Transmission

The motor models are based on the well known equations describing a dc motor:

(1.3) $$\begin{cases} V = RI + L\dfrac{dI}{dt} + K_E\omega(t) \\ \tau^M = K_T I = (J_m + J_l)\dfrac{d\omega(t)}{dt} + B\omega(t) + \tau_f + \tau_{gr} \end{cases}$$

where L = coil inductance [H]; R = armature resistance [Ω]; V = input voltage [V]; J_m = rotor moment of inertia [Kg m2]; J_l = moment of inertia of the load [Kg m2]; B = viscosity coefficient [N s m-1]; K_T = torque constant [N m A-1]; K_E = back EMF constant [V s rad-1]; τ^M is the torque directly provided by the motors; τ_f is the friction torque, and τ_{gr} is the torque provided by the gravity.

Known the values of the electrical and mechanical constants of every motor, by integrating equations (1.3), motor current I and the motor output torque τ^M for each of the motors are calculated, given an input voltage V. This is the way the four motors M1-M4 of James arm are commanded. Given our software setup, the torques produced by the motors must be converted into the torques applied to the kinematic chain. As previously stated, this follows from the fact that most of the motors collaborate in moving the same joint, as sketched in Fig. 4.
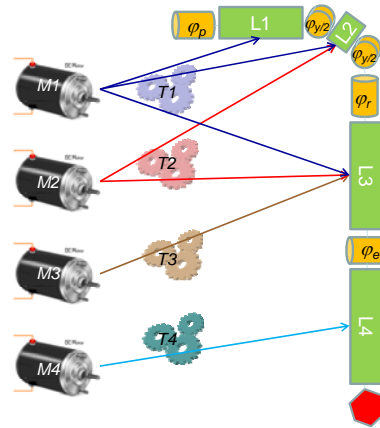

Fig. 4 Sketch of the mechanical transmission layout. Angles are referred to the joints positions.

1) Torque Conversion:

We here describe how motor torques τ^M are converted into joint torques τ^S.

According to (1.1), $\varphi^J = D\varphi^M$, this conversion can be performed by means of a change of coordinates, thus obtaining $\tau^J = D^{-T}\tau^M$.

More explicitly, from the dynamics of the Lagrangian system:

$$(1.4) \qquad \tau^J = M(\varphi^J)\ddot{\varphi}^J + C(\varphi^J, \dot{\varphi}^J)\dot{\varphi}^J + N(\varphi^J, \dot{\varphi}^J)$$

easy computation leads to:

$$(1.5) \quad D^T(\tau^J) = \hat{\tau}^J = \hat{M}(\hat{\varphi}^J)\ddot{\hat{\varphi}}^M + \hat{C}(\hat{\varphi}, \dot{\hat{\varphi}})\dot{\hat{\varphi}}^M + \hat{N}(\hat{\varphi}, \dot{\hat{\varphi}}) = \tau^M$$

In order to take in account the frictional contributes which affects the mechanical transmission lines from the motors to the joints, the simulator reproduces four transmission T1, T2, T3, T4 which brings the mechanical power from the converters output (the dc motors shaft after the gearhead) to the links. Each transmission is affected by power losses due to the presence of friction, modeled like a pure viscous friction. The modeled friction originally derives from the motion of each link according to the equation:

$$(1.6) \qquad \tau_F = E\dot{\varphi}^J$$

where $\dot{\varphi}^J$ is the time derivative of the joint angular position vector and E is the diagonal matrix of the estimated viscous friction coefficients expressed in [Ns/rad]:

$$(1.7) \qquad E = \begin{bmatrix} 9.8 & 0 & 0 & 0 \\ 0 & 10.2 & 0 & 0 \\ 0 & 0 & 2.5 & 0 \\ 0 & 0 & 0 & 2.8 \end{bmatrix}$$

Then, according to (1.6), introducing friction terms, the resulting torque applied to the ith link can be finally calculated as:

$$(1.8) \qquad \tau^J = D^{-T}\tau^M - \tau_F$$

C. Motion controller

The Motion Controller is aimed at driving the motors to move the robot arm according to a series of constraints on kinematics, dynamics and efficiency, which are determined by the given mission. It is composed of two stages: the pre-motion stage and the motion control stage. In the pre-motion stage the user can define the mission of the arm in terms of duration, initial and boundary conditions of the motion, energy parameters. Then, the system calculates the reference trajectories for the arm, i.e. the trajectories that the arm should carry out in order to accomplish the given mission. These trajectories are evaluated as solutions to optimal control

problems which are chosen by the user among a set of four different control strategies which will be detailed herein.

In the motion stage of the controller, the reference trajectories expressed in joint coordinates φ^J_{ref} are compared to the actual position φ^J_i of the joints by a PID regulator. From this comparison, the motion control stage provides the motors with appropriate values of input voltage V to the aim of driving the arm along the trajectories of reference. In the following Fig. 5 the working principles of the controller module are shown.
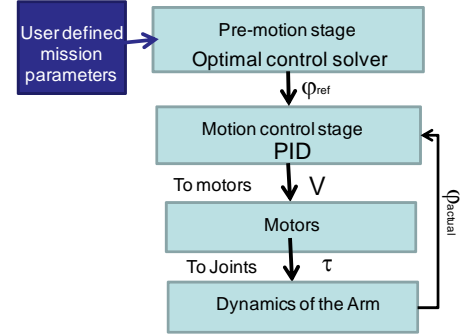

Fig. 5 Scheme of the Motion Controller module.

The Motion Controller needs to calculate both the inverse and the forward kinematic of the system. Because of the kinematic redundancy of the 4DOF arm, the solution of the inversion problem is not unique, therefore we chose to adopt an inversion techniques based on the downhill simplex method of Nelder and Mead (30), which we developed in C language and plugged into the simulator.

The four control strategies that have been developed are the Minimum Jerk in the joint space (relative angular coordinates of the joints) which is currently used in the real James robot, the Minimum Jerk in the Cartesian space (Cartesian end-effector position referred to the inertial base frame S – Fig. 2), the Minimum Torque and the Minimum Torque change. All these controls can be described as solutions of an optimal control problem subject to the minimization of a cost function.

Formally, a typical optimal control problem can be represented as:

$$(1.9) \quad \begin{cases} \min_u \quad J = \int_{t_0}^{t_f} \xi(x(t), u(t), t)dt \\ \text{subject to } \begin{cases} \dot{x}(t) = f(x(t)) + g(x(t))u(t) \\ x(t_0) = x_0 \end{cases} \end{cases}$$

where ξ is the cost function to minimize with respect to the control system variable $u(t)$, and $x(t)$ is variable describing the state of the system. The Motion control module calculates the values of $u(t)$ that minimize the functional, and the state of the system accordingly. Then, the values $x(t) = (\varphi^J(t), \dot{\varphi}^J(t))$ deriving from the minimization process are used as reference trajectories that the arm will have to follow.

The aforesaid four control strategies present different forms of the functional ξ.

The Minimum Jerk in Cartesian or end effector space (MJe) has the functional equal to:

$$(1.10) \quad \xi\left(x(t), y(t), z(t)\right) = \left(\frac{d^3x}{dt^3}\right)^2 + \left(\frac{d^3y}{dt^3}\right)^2 + \left(\frac{d^3z}{dt^3}\right)^2$$

where (x, y, z) are the hand effector coordinates. Similarly, the Minimum Jerk in joint space coordinates (MJq) is characterized by:

$$(1.11) \quad \xi\left(\boldsymbol{\varphi}(t)\right) = \left(\frac{d^3\boldsymbol{\varphi}}{dt^3}\right)^2$$

Where $\boldsymbol{\varphi}$ is the vector of the joint coordinates. As for MJe, the peculiarity of this problem is that it is possible to find a close form solution, which can be used to speed up the trajectories calculation or to compare the solver results with a known solution. The cost of the Minimum Jerk model is purely kinematic and it does not take in account dynamical arm parameters like mass, external forces, etc. The Minimum Torque Change (MTC) function indeed is related with total torque change during the movement, which is given by:

$$(1.12) \quad \xi\left(\boldsymbol{\tau}(t)\right) = \left\|\frac{d\boldsymbol{\tau}}{dt}\right\|^2$$

where $\boldsymbol{\tau}$ is the vector of torques acting on the joints. Likewise the minimum jerk cost, the final time of the action has to be specified, that is the system is bound to reach the target within a specified time.

Similarly to the MTC, this control takes in account the arm dynamics as it is aimed at minimizing the torque provided to the joints. The Minimum Torque (MT) cost function is given by:

$$(1.13) \quad \xi\left(\boldsymbol{\tau}(t)\right) = \left\|\boldsymbol{\tau}\right\|^2$$

where $\boldsymbol{\tau}$ is the vector of torques acting on the joints.

D. Energy Analysis module

This module is designed to provide the information relative to the energy flows occurring inside the energy chain, it collects the energy relevant parameters within specified subsystems or control volumes, and within a given observation time. More specifically, the following control volumes have been identified (Fig. 6): single motor; motors group; power transmission of a single motor; overall power transmission; single link of the arm; links group (complete robot arm); whole system.

The power supplier unit is, by virtue of its operating criteria, a strictly one-way energy converter. On the other hand the energy inside the rest of the chain passes through the components in both directions: it flows towards the links and, in principle, it can return back towards the mechanical transmission up to the power supplier. This may happen, for example, during some particular arm movements under the effect of external forces, such as the weight of a load held by the robot, or the gravity acting on the arm. Furthermore, in dependence of on the observation time, the above described motor coupling may cause some of the motors to be crossed

by an energy flow going backwards from the links to the power supplier, whereas the control volume comprising all the motors acting on such link may be crossed by an energy flow in the opposite direction, that is from the power supplier to the links. Hence, due to the mechanical coupling of the converters, it may happen, that given a particular mission and a control time, some of the converters acts like motors, while others behave like voltage generators.
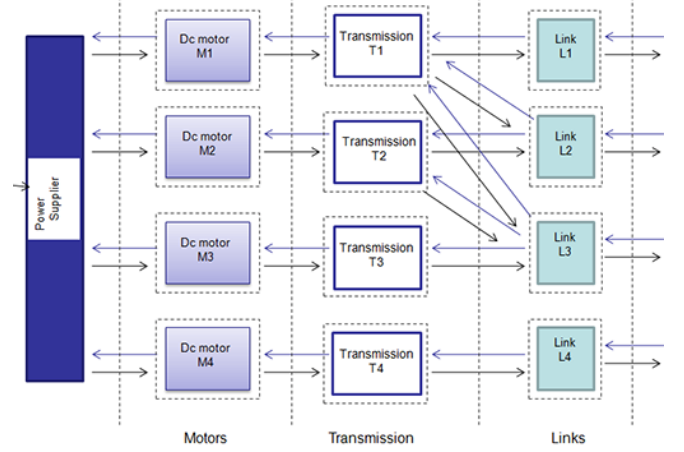

Fig. 6 Diagram of the energy chain. Control volumes are evidenced by dashed lines.

Consequently, in order to calculate the energy balance of the energy chain elements, as well as of the whole chain, it is essential to take particular care in defining the energy parameters which characterize the each control volume.

In view of that, let's consider a volume of control crossed by energy flows in both directions in which there are energy losses. Conventionally, the converter input facing the primary source is established as being the "input" frontier while the "output" frontier is the one facing the end-user. However, depending on the control time, the overall flow of energy crossing the volume of control may flow from the "input" to the "output", or vice versa. If this control volume enclosed one of the M1-M4 converters, in the first case such converter would act as a motor, while in the second case it would act as a power generator. In consideration of this, we define the "input" of a given volume of control as the frontier from which the net energy flow, calculated over the whole control time, enters the volume, and the "output" as the frontier crossed by the energy flow leaving such volume.

With reference to Fig. 7, given a control time T and a volume of control having frontiers 'p' and 'q' we define net energy flows as:

$$(1.14) \quad W^p = (W^p)_f - (W^p)_b \ , \ W^q = (W^q)_f - (W^q)_b$$

where: $(W^p)_f$ = forward energy to 'p'; $(W^q)_f$ = forward energy to 'q'; $(W^p)_q$ = backward energy from 'p'; $(W^q)_b$ = backward energy from 'q'.

According to the present definitions, the frontier 'p' will be called 'input' frontier, while 'q' will be called the 'output' frontier of the volume of control. It is now possible to

unambiguously define the expressions of efficiency associated to a determined control volume and a determined control period.
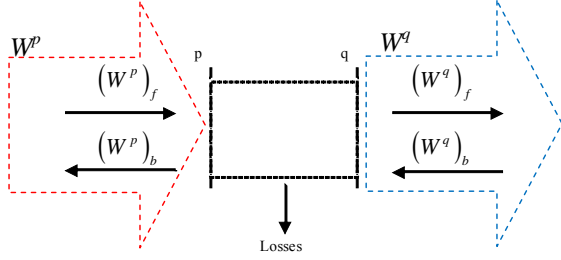

Fig. 7 Two-way energy converter

The following expressions of "forward" $(\bar{\eta})_f$ and "backward" $(\bar{\eta})_b$ average converter efficiency are applicable when the energy flow across the converter is time-dependent and its internal energy is negligible as compared to the flow passing through in the control time:

$$(1.15) \qquad (\bar{\eta})_f = \frac{(W_{out})_f}{(W_{in})_f}$$

$$(1.16) \qquad (\bar{\eta})_b = \frac{(W_{in})_b}{(W_{out})_b}$$

The effective average efficiency of the converter is defined as:

$$(1.17) \qquad \bar{\eta} = \frac{(W_{out})_f - (W_{out})_b}{(W_{in})_f - (W_{in})_b}$$

The backward energy ratio R is defined as the ratio between the backward energy module returning up to the converter from the output frontier and the direct energy output:

$$(1.18) \qquad R = \frac{|(W_{out})_b|}{(W_{out})_f}$$

From (1.17) and (1.18), the generalized form of the average efficiency of the i-th converter is:

$$(1.19) \qquad \bar{\eta}^i = \frac{1 - R^i}{1 - R^i \left(\bar{\eta}^i\right)_f \left(\bar{\eta}^i\right)_b} \left(\bar{\eta}^i\right)_f$$

Equation (1.19) shows clearly that the efficiency of the converter does not depend on its intrinsic performances only, i.e. forward and backward efficiency, but also on the backward energy ratio R, i.e. on the way the converter is used: the more energy is returning, the less the converter is in fact efficient, either it behaves like a motor either like a generator.

In the light of the aforementioned concepts, the energy behaviour of the energy chain has been derived by integrating over time the estimated power flowing through each component (dc motors, transmission, links).

Considering (1.20), from the left to the right we have the equations for input power to motor M_i, output power of the motor M_i, output power of the transmission T_i, and output power of the link L_i.

$$(1.20) \quad P_{in}^{Mi} = V_{Mi}I_{Mi} \; ; \; P_{out}^{Mi} = \tau^{Mi}\dot{\varphi}^{Mi} \; ; \; P_{out}^{Ti} = \tau^{Ti}\dot{\varphi}^{Mi} ; \; P_{out}^{Ji} = \tau^{Ji}\dot{\varphi}^{Ji}$$

The quantities V_{Mi} and I_{Mi} are the input voltage to motor M_i and the current circulating into M_i respectively, while τ^{Ti} is the torque exerted by transmission T_i. We also considered that P_{out}^{Mi} is equal to the input power to transmission T_i (Fig. 6).

This model allowed to locate and estimate the energy losses taking place in the system as well as to identify when energy recover may occur. Furthermore, such parameterization allowed to study the effects of the robot mechanical design upon each single component efficiency as well as on the overall system efficiency.

V. VALIDATION

The validation of the present simulator has been conducted in four phases: the parametric identification of the motors running inside the James arm, the tuning of the simulated motors on the base of the measured data, the observation of the dynamic of the arm during a set of simple movements and the tuning of the friction affecting the motors transmissions inside the robot James. Furthermore, a series of tests have been yielded on the software model deputed to the calculation of the optimal control trajectories (JOCS), by comparing it with a state of the art solver.

VI. SIMULATED MISSIONS AND ENERGY BALANCE

The simulated missions consisted in reaching tasks, in compliance of predefined constraints in time, space and forces. Each goal oriented task has been repeated for each of the four above described control strategies. The tests has been run on the following sets of missions:
- Mission 0, single phase motion: the robot performs one single reaching movement from the rest position to the target.
- Mission 1, multiple phase motion on the horizontal plane: six targets have been positioned in from of the robot. All of them lay on the same horizontal plane, three on a proximity position and three on a distal position (Fig. 8).
- Mission 2, multiple phase motion on the vertical direction: five different targets have been positioned in front of the robot and distributed in space along vertical trajectories. Two of them were situated in the lateral position, and three between a frontal-proximal and frontal-distal position.
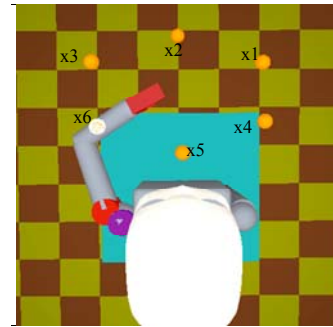

Fig. 8 Mission 1: targets laying on the horizontal plane in front of the robot.

All the main electrical and mechanical parameters have been calculated at a sample rate of 50 kHz, in order to include the high frequencies dynamics of the electrical signals

occurring inside the converters. The physical simulation required a variable time step integrator for stiff equations (ode23 Rosembrock) with integration step not lower than 10 kHz. Such high sampling frequency, in association with the complicated architecture of the simulator, required a large amount of CPU time on robust workstations (Intel Core 2 Duo processors at 2.4 GHz, 4 GB RAM memory). Finally, starting from a complete report of the motors activity provided by the simulator, all the tests have been analysed from the kinematics, the dynamics and the energetic point of view.

Herein we present some detailed information on Mission 2, where, starting from a position proximal to the torso (rest position x5 of Table I), the robot reaches the set of six different targets, stopping for a period of t=0.35s in correspondence of each target. Each path is performed both in the onward and in the backward direction in order to form a series of closed loops. The total simulation time is T=60s, being every path covered in 5s. In the following table the target positions are summarized.

TABLE II
SIMULATED MISSION N. 2, TARGETS POSITIONS

Target Positions - Cartesian space [m]	Target Positions – joint space (Inverse Kinematics) [rad]	Reaching time T_{tgt} [s]
x1=(-0.02, 0.58, -0.39)	$\varphi1 = (0.78, 0.24, 0.001, -0.88)$	[15; 55]
x2 =(-0.18, 0.58, -0.42)	$\varphi2 = (0.84, -0.01, 0.16, -0.89)$	[5]
x3=(-0.35, 0.58, -0.39)	$\varphi3 = (0.79, -0.19, 0.02, -0.87)$	[25;35;45]
x4=(-0.02, 0.58, -0.21)	$\varphi4 = (0.46, -0.02, 0.96, -1.76)$	[40]
x5=(-0.18, 0.58, -0.17)	$\varphi5 = (1.05, -0.49, 1.73, -2.18)$	[0;10;20;30]
x6=(-0.35, 0.58, -0.21)	$\varphi6 = (0.65, -0.70, 1.17, -1.80)$	[50;60]
Path: x5 → x2 → x5 → x1 → x5 → x3 → x5 → x3 → x4 → x3 → x6 → x1 → x6		

As far as Mission n. 2 kinematics is concerned, Fig. 9 shows the robot hand trajectories in the Cartesian space, depending on the four controls MJe, MJq, MT and MTC. The 3D graph is reported together with a projection on orthogonal planes XY. From the 3D graph and its projection on the XY plane of Fig. 9, it clearly appears that only the Minimum Jerk on the end effector (MJe) space keeps the hand on the horizontal plane, where the targets are lying, while the other controls cause the hand to raise over the plane. Furthermore it can be noticed that MJe produces straight lines both in the onward and in the backward path, whereas MJq follows a slightly curved path either in the XZ and in the YZ plane, which has an estimated maximum distance from the straight line of about 8 cm.

MTC trajectories in the Cartesian space are similar to the MJq curves but they shows more arched paths and, in some cases, a weak dependency on the direction of the motion.

The reference trajectories calculated by the Minimum Torque control provide the most curved paths, with trajectories which depend on the direction of motion. It should be noticed that, being the MJe and MJq pure kinematic controls, the calculated trajectories are exactly the same in the two direction of motion, whereas the MT and MTC are influenced by the dynamics of the robot, including the external forces acting on the physical system, like gravity and

friction which modify the pure kinematic-based symmetry of the onward and backward curves. It is also interesting to point out that, even if moving the hand above the horizontal plane on which the targets lay requires an additional torque to push the arm against the gravity, the solutions provided by the Minimum Torque Change and the Minimum Torque give evidence of this dynamic.
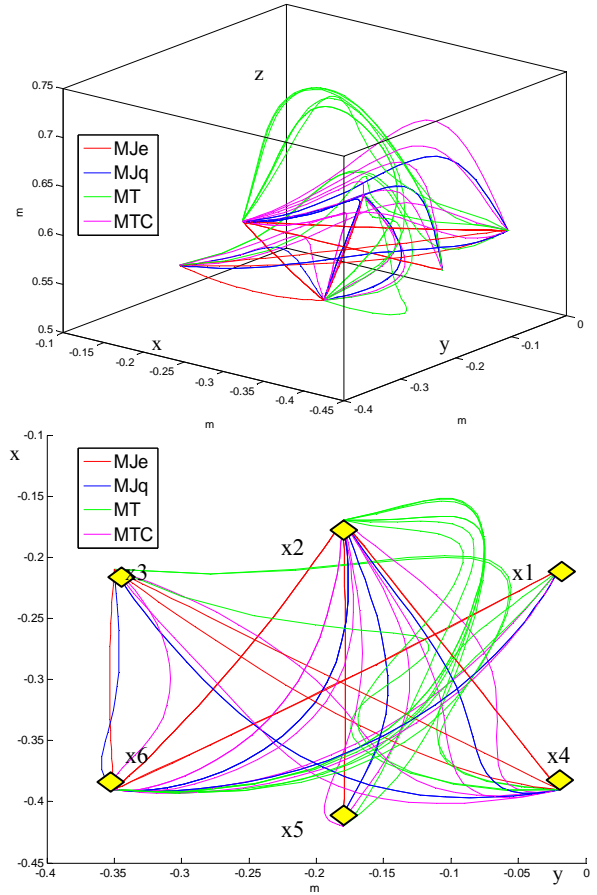

Fig. 9 Hand trajectories in the Cartesian space calculated by the four controls MJe, MJq, MT and MTC. 3D plot (upper) and its XZ plane orthogonal projection (lower plot).

As far as the energy balance is concerned, following Table III summarizes the most relevant energy parameters calculated during the execution of Mission 2. All the values are estimated with respect to a control time equal to the mission period, that is t=60s.

TABLE III
SIMULATED MISSION N. 2, BOUNDARY CONDITIONS

	MJe	MJq	MTC	MT
Energy parameters				
M1 Efficiency η_{m1}	0.20	0.16	0.16	0.30
M2 Efficiency η_{m1}	0.12	0.12	0.12	0.07
M3 Efficiency η_{m1}	0.19	0.18	0.18	0.16
M4 Efficiency η_{m1}	0.18	0.19	0.19	0.17
Transmission Efficiency η_{t1}	0.57	0.57	0.55	0.50
Transmission Efficiency η_{t2}	0.33	0.49	0.50	0.58
Transmission Efficiency η_{t3}	0.51	0.49	0.50	0.51

Transmission Efficiency η_{t4}	0.52	0.51	0.52	0.52
M1 Backward energy ratio	0.38	0.229	0.237	0.049
M2 Backward energy ratio	0.691	0.568	0.551	0.765
M3 Backward energy ratio	0.192	0.067	0.058	0.072
M4 Backward energy ratio	0.003	0.002	0.002	0.011
T1 Backward energy ratio	0.537	0.380	0.408	0.136
T2 Backward energy ratio	0.876	0.735	0.719	0.802
T3 Backward energy ratio	0.201	0.083	0.070	0.082
T4 Backward energy ratio	0.026	0.016	0.016	0.066
Total system efficiency	0.095	0.089	0.088	0.102
Tot Backward energy ratio	0.036	0.045	0.033	0.011

Considering the most relevant energy related parameters which have been calculated during Missions 1 and 2, we can infer that the highest system efficiency is provided by the Minimum Torque control (MT). Similarly, it has been calculated that the worst average efficiency derives from Minimum Torque Change (MTC) and Minimum Jerk in joints coordinates (MJe). They provide quasi identical values, about 15% lower than MT (Fig. 10).

However, MT, together with MJe, seems to be the most energy consuming control, since it requires roughly 20% more energy than MJq and MTC (Fig. 11). It is also noteworthy that MT produces the worst trajectories considering the goal of the missions. Indeed, MT, trajectories in the Cartesian space are noticeably curved and widely diverging from a desirable straight line path. On the other hand, it has been estimated that the control strategy producing the best trajectories, always with respect to their linearity, is MJe, which shows a higher efficiency than MTC and MJq, but requiring more energy.
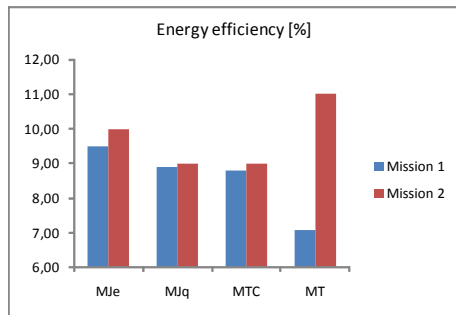

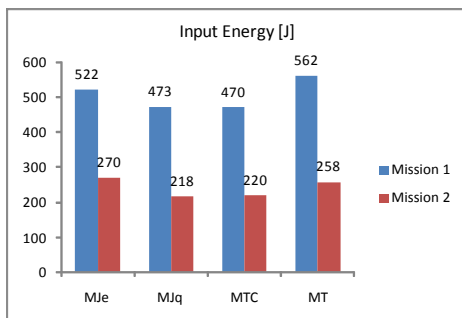Fig. 10 average chain efficiencies calculated for missions 1 and 2

Fig. 11 Input energy to the system, calculated for missions 1 and 2

VII. CONCLUSIONS

According to the simulation results, the control strategy currently implemented on the real robot James (i.e. MJq)

seems to be poorly efficient. Moreover, the average backward energy ratio of MJq (Fig. 12) calculated for both the two missions, is maximum for MJq. Thus, at least in principle, MJq may assure the largest amount of energy recovery, provided that appropriate accumulators and hardware adaptations are added to the real robot.

This first study is aimed at exploring a possible approach for helping the understanding of the energy balance of robots in correlation with their motion controls and their mechanical constraints. Further studies on this topic might, for example, conduct to the design of energy recovery systems and to the exploration of energy efficient motion strategies.
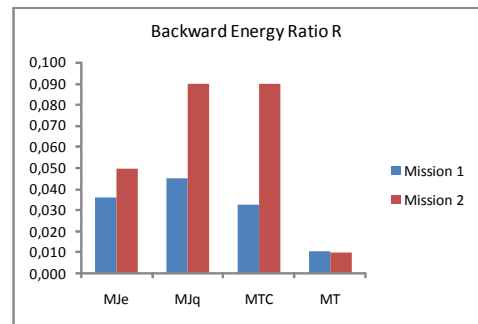

Fig. 12 Average system efficiencies calculated for missions 1 and 2

REFERENCES

[1] O. Khatib et al., *Robots in Human Environments*. Stanford University. 2000.
[2] W. Schiehlen, "Energy-optimal design of walking machines", *Multibody System Dynamics*, pp. 129-141, 2005.
[3] I. Ieropoulos, C. Melhuish, W. Aberystwyth "Imitating Metabolism: Energy Autonomy in Biologically Inspired Robotics", *Proc. of the AISB '03*, 2003, pp. 191-194.
[4] E. Todorov, "Optimality principles in sensorimotor control", *Nature Neuroscience*, Vol. 7, p. 907-915.
[5] A. Pini-Prato, M. Repetto, G. Vandelli, "Hybrid-series vehicle mathematical simulation model", *Trans. of the Wessex Institute IX*, 2003.
[6] G.L Berta, A. Pini Prato, "Series-Hybrid Power Trains: Design Criteria", *Proc. XXV FISITA Congress*, BiJin 1994.
[7] G.L. Berta, A. Pini Prato, Bolfo F., "On Road Testing Hybrid Vehicles", *Int. Symp. on Automotive Technology and Automation*, 1993.
[8] E. Todorov et al., "Optimal control methods suitable for biomechanical systems", *Proc. of the 25th Annual International Conference of the IEEE Engineering in Biology and Medicine Society,* 2003.
[9] Y. Mei et al. "Deployment strategy for mobile robots with energy and timing constraints". *Proc. of the IEEE International Conference on Robotics and Automation,* Barcelona, 2005. pp. 2816–2821.
[10] M. Kawato, "Internal models for motor control and trajectory planning", *Current Opinion in Neurobiology*, pp. 718-727, 1999.
[11] L Jamone, G Metta, F Nori, G Sandini "James: A Humanoid Robot Acting over an Unstructured World"- *Humanoid Robots*, 6th IEEE-RAS International Conference, 2006.
[12] S. Collins, A. Ruina, R. Tedrake, M. Wisse "Efficient Bipedal Robots Based on Passive-Dynamic Walkers", *Science,* vol. 307, 1082 , 2005.